Hyperentanglement-enhanced quantum illumination

Ashwith Varadaraj Prabhu [1], Baladitya Suri [2] and C. M. Chandrashekar[2,3]
[1]*Indian Institute of Science, Bengaluru 560012, India*
[2]*Department of Instrumentation & Applied Physics, Indian Institute of Science, Bengaluru 560012, India*
[3]*The Institute of Mathematical Sciences, Chennai 600113, India*

(Received 26 October 2020; revised 6 May 2021; accepted 6 May 2021; published 17 May 2021)

In quantum illumination, the signal mode of light, entangled with an idler mode, is dispatched towards a suspected object bathed in thermal noise, and the returning mode, along with the stored idler mode, is measured to determine the presence or absence of the object. In this process, entanglement is destroyed but its benefits in the form of classical correlations and enlarged Hilbert space survive. Here, we propose the use of a probe state *hyperentangled* in two degrees of freedom, polarization and frequency, to achieve a significant 12-dB performance improvement in the error probability exponent over the best-known quantum illumination procedure in the low-noise regime. We present a simple receiver model using four optical parametric amplifiers (OPAs) that exploits hyperentanglement in the probe state to match the performance of the feed-forward sum-frequency generator (FF-SFG) receiver in the high-noise regime. By replacing each OPA in the proposed model with a FF-SFG receiver, a further 3-dB improvement in the performance of a lone FF-SFG receiver can be seen.

DOI: 10.1103/PhysRevA.103.052608

I. INTRODUCTION

Detecting the presence or absence of an object in real space using low-intensity probe states is often a challenging task due to the surrounding thermal noise. In such an object-detection scenario, protocols using quantum states as probes have been developed, where a probe state is transmitted towards the suspected object and the returning state is measured. The efficacy of different transmitter-receiver models is quantified using the probability of error in detecting the presence or absence of the suspected object [1,2]. For a given transmitter, the minimum error probability for deducing the object to be present is achieved when the measurement projects onto the positive eigenspace of $\rho_1 - \rho_0$, where ρ_0 is the density operator of the returning state in the absence of any object while ρ_1 is the density operator in its presence [3]. The calculation of this minimum error probability is, in general, prohibitively difficult. The relatively tractable quantum Chernoff bound (QCB) provides an asymptotically tight bound on the error probability (p_e) [4]. It is defined as $Q_{\mathrm{QCB}} \equiv \min_{0\leqslant s\leqslant 1} \mathrm{Tr}[\rho_1^s \rho_0^{1-s}]$. After N detection events, the bound on the error probability is given by

$$p_e^{(N)} \leqslant \tfrac{1}{2}(Q_{\mathrm{QCB}})^N. \tag{1}$$

Several candidate probe states, viz., coherent states, single photons [5], entangled biphotons, and the two-mode squeezed vacuum (TMSV) state, have been considered for object detection [6]. Quantum illumination (QI), in general, refers to the use of entangled states, where photons in one of the entangled states, treated as signal photons, are sent towards the suspected object, and the so-called idler photons in the other entangled state are kept back. Joint measurement of the returning photons and idler photons has been shown to be more effective than the use of classical states of light in detecting the presence or absence of the object in certain parameter regimes. With the mean number of thermal photons denoted by N_B and the reflectance of the object by κ, the quantum Chernoff bound for QI using an entangled probe state such as TMSV, having N_S mean number of photons in each entangled mode, was computed [6] and a 6-dB (factor-of-4) improvement in the exponent of the error bound over the best classical object detection strategy was shown in the high-noise and low-signal-intensity regime ($N_S \ll 1$, $\kappa \ll 1$, and $N_B \gg 1$) [6,7]. After N iterations, this bound is given by [6]

$$p_{e,\mathrm{QI}}^{(N)} \leqslant e^{-\kappa N N_S/N_B}/2. \tag{2}$$

The low-noise regime, on the other hand, is characterized by the mean thermal photon number per temporal mode (N_B) being significantly less than unity ($N_B \ll 1$). In a typical QI protocol in this regime, a transmitter dispatches N iterations of signal photons spanning over M temporal modes ($M \gg 1$) towards a possible target of very poor reflectance κ. In the so-called "bad regime" [5] characterized by $MN_B \ll 1$ and $\kappa \ll N_B/M$ within the low-noise regime, the bound on the error probability is given by [8]

$$p_{e,\mathrm{QI}}^{(N)} \leqslant e^{-NM\kappa^2/8N_B}/2, \tag{3}$$

which is lower by a factor of M in the exponent than a detection protocol employing only a single-photon probe (SP) [8],

$$p_{e,\mathrm{SP}}^{(N)} \leqslant e^{-N\kappa^2/8N_B}/2. \tag{4}$$

However, it should be noted that the use of a coherent state as the probe (CS), which has an associated error

probability bound of $e^{-\kappa N_S}/2$, outperforms QI in this regime [8]. At the heart of it, the improved performance of QI stems from the larger Hilbert space of the entangled signal-idler system [9]. Therefore, the use of an enlarged Hilbert space through "hyperentanglement," i.e., entanglement in more than one degree of freedom of the probe, without increasing the number of photons [10] along with an appropriately designed receiver can further increase the efficiency of QI. With various experiments demonstrating the generation of hyperentangled states of photons [11], its use for QI can be substantiated. While the enhancement effected by hyperentanglement in a continuous parameter estimation problem has been analyzed in an earlier work [12], this article shines light on the enhancement in what is essentially a hypothesis testing task. In this article, we propose object detection using a probe state hyperentangled in polarization as well as frequency degrees of freedom [13]. We show that the QCB for object detection using hyperentangled photons gives a remarkable 12-dB improvement in the exponent of the error probability over QI in the "bad regime." For the receiver, we propose a setup that includes four optical parametric amplifiers (OPAs) that exploits the presence of correlations between the four pairs of modes for every iteration due to the hyperentanglement. This results in a 3-dB improvement in the high-noise regime over the earlier proposals for practical quantum illumination receivers using the optical parametric amplifier (OPA) and a phase conjugate receiver (PCR) [14,15]. This performance matches the only other proposal that theoretically achieves the same using sum-frequency generation receiver with a feed-forward (FF-SFG) receiver [16], whose implementation is, to our knowledge, more challenging. Finally, by replacing each OPA with a FF-SFG receiver, we also show that this hyperentanglement-enhanced FF-SFG receiver outperforms the lone FF-SFG receiver by 3 dB in the error probability exponent. The next section details the 12-dB performance improvement offered by hyperentanglement in the low-noise regime and the two sections following the next analyze the performance of the proposed hyperentanglement-enhanced OPA receiver and the hyperentanglement-enhanced FF-SFG receiver in the high-noise regime.

II. HYPERENTANGLEMENT-ENHANCED SENSITIVITY IN THE LOW-NOISE REGIME

Ever since the first experimental demonstration of the generation of hyperentangled photon pairs [17], different procedures to generate hyperentanglement in different degrees of freedom of photons have been successfully demonstrated. Here, we will briefly outline one such procedure [13] to generate states hyperentangled in polarization and frequency degrees of freedom. Using two identical type-II noncollinear spontaneous parametric down-conversion (SPDC) generators driven by identical pumps, derived from a common pump, $|\Phi\rangle_1$ and $|\Phi\rangle_2$, that are entangled in a polarization degree of freedom [18] are produced. For each of these states, the mean number of photons in each entangled mode of the state is N_S'. The states have the Fock state representation [19],

$$|\Phi\rangle_1 = \sum_{n=0}^{\infty} \frac{N_S'^{n/2}}{\sqrt{2}(N_S'+1)^{(n+1)/2}} (|n\rangle_{1,H,S}\,|n\rangle_{1,V,I} + |n\rangle_{1,H,I}\,|n\rangle_{1,V,S}), \tag{5}$$

$$|\Phi\rangle_2 = \sum_{n=0}^{\infty} \frac{N_S'^{n/2}}{\sqrt{2}(N_S'+1)^{(n+1)/2}} (|n\rangle_{2,H,S}\,|n\rangle_{2,V,I} + |n\rangle_{2,H,I}\,|n\rangle_{2,V,S}). \tag{6}$$

Here, S and I refer to the signal and idler frequency, 1 and 2 denote distinct spatial modes, while H and V denote horizontal and vertical polarization, respectively. The output spatial modes of a single noncollinear SPDC process are distinct but using appropriate lenses, the spatial overlap of the output modes can be increased such that the two spatial modes may be approximated to be identical. Thus, the signal and the idler frequency modes occupy the same spatial mode. If the original common pump had been used to drive a single SPDC generator, the mean number of photons in each of the two output modes would have been N_S (say) and would be related to N_S' as $N_S' = N_S/2$. The two spatial modes form the input to a balanced beam splitter to give

$$a_3 = \frac{a_1 + ia_2}{\sqrt{2}}, \tag{7}$$

$$a_4 = \frac{ia_1 + a_2}{\sqrt{2}}. \tag{8}$$

The resulting state is entangled in frequency ω_S and ω_I besides polarization. A first-order approximation in the squeezing parameter of the resulting hyperentangled state and setting the relative pump phase to zero or π yields a hyperentangled biphoton state [13]. For the low-noise regime, the time-bandwidth product is adjusted such that the transmitter pulse spans over M temporal modes to give the following output state [13],

$$|\Psi\rangle_{3,4} = \frac{1}{2\sqrt{M}} \sum_{k=1}^{M} [|1_k\rangle_3\,|1_k\rangle_4 \otimes \{|H\rangle_3\,|V\rangle_4 + |H\rangle_4\,|V\rangle_3\} \otimes \{|\omega_S\rangle_3\,|\omega_I\rangle_4 + |\omega_S\rangle_3\,|\omega_I\rangle_4\}]. \tag{9}$$

The subscripts 3 and 4 indicate the two distinct spatial modes while $|1_k\rangle_j$ represents the presence of a single photon in the kth temporal mode and the spatial mode j and none in the other temporal modes. One of the entangled photons is sent towards the possible target while the other is stored. Let the spatial mode associated with the dispatched photon be 3 and the spatial mode occupied by the stored photon be 4. The local state of the stored photon is of the form

$$\sigma = \mathrm{Tr}_3(|\Psi\rangle\,\langle\Psi|_{3,4}) = \frac{I_4}{4M}, \tag{10}$$

where I_4 is the $4M$-dimensional identity operator over the space spanned by the single-photon states occupying M distinct temporal modes, with each mode being further indexed by two distinct frequencies and polarizations. In the absence of any object, the returning state is the unpolarized thermal

state with a mean number of thermal photons per temporal mode (N_B) satisfying the condition $MN_B \ll 1$. The mean number of thermal photons depends on the frequency but assuming the values of ω_S and ω_I are sufficiently close, we approximate the mean thermal photon number to be the same for both the frequencies. The thermal state ρ_t under the low-noise condition is approximated as [5]

$$\rho_t = (1 - MN_B)\,|0\rangle\langle 0|_3 + \frac{N_B}{4}\sum_{k=1}^{M}[|1_k\rangle\langle 1_k|_3 \otimes \{|H\rangle\langle H|_3 + |V\rangle\langle V|_3\} \otimes \{|\omega_S\rangle\langle\omega_S|_3 + |\omega_I\rangle\langle\omega_I|_3\}] \tag{11}$$

$$= (1 - MN_B)\,|0\rangle\langle 0|_3 + \frac{N_B}{4} I_3. \tag{12}$$

Here, I_3, as I_4, is an identity operator over the single-photon subspace. In a slight abuse of notation, we have indexed the returning state as well as the dispatched single-photon state by 3. In the absence of any object, the global state ρ_0 (i.e., returning state+stored state) is

$$\rho_0 = \rho_t \otimes \sigma. \tag{13}$$

In the presence of a weakly reflecting object with reflectance κ, we have

$$\rho_1 = (1-\kappa)\rho_0 + \kappa\,|\Psi\rangle\langle\Psi|_{3,4}\,. \tag{14}$$

The minimum error probability for distinguishing between ρ_0 and ρ_1 is bounded by the quantum Chernoff bound [20]. In order to determine QCB, we need to evaluate ρ_0^{1-s} and ρ_1^s,

$$\rho_0^{1-s} = \left[(1 - MN_B)^{1-s}\,|0\rangle\langle 0|_3 + \left(\frac{N_B}{4}\right)^{1-s} I_3\right] \otimes \frac{I_4}{(4M)^{1-s}}, \tag{15}$$

$$\rho_1^s = (1-\kappa)^s(1 - MN_B)^s\,|0\rangle\langle 0|_3 \otimes \frac{I_4}{(4M)^s} + (1-\kappa)^s\left(\frac{N_B}{16M}\right)^s (I_3 \otimes I_4 - |\Psi\rangle\langle\Psi|_{3,4}) + \left[(1-\kappa)\frac{N_B}{16M} + \kappa\right]^s |\Psi\rangle\langle\Psi|_{3,4}\,. \tag{16}$$

In arriving at the preceding two equations, we have used the fact that the vacuum state is orthogonal to the single-photon subspace and that $(I_3 \otimes I_4 - |\Psi\rangle\langle\Psi|_{3,4})$, in addition to being orthogonal to the vacuum state, is also orthogonal to $|\Psi\rangle\langle\Psi|_{3,4}$. Taking the trace of $\rho_0^{1-s}\rho_1^s$ yields

$$Q_{\mathrm{QCB}} = \min_{0\leqslant s\leqslant 1}(1-\kappa)^s\left\{1 + \frac{N_B}{16M}\left[-1 + \left(1 + \frac{16\kappa M}{(1-\kappa)N_B}\right)^s\right]\right\} \tag{17}$$

$$= \min_{0\leqslant s\leqslant 1}\left\{1 - \kappa s + \frac{N_B}{16M}\left[-1 + \left(1 + \frac{16\kappa M}{N_B}\right)^s\right]\right\} + O(N_B^2, \kappa N_B). \tag{18}$$

We now focus on the so-called bad regime, which is characterized by $MN_B \ll 1$ and $\kappa \ll N_B/M$. The second condition allows us to approximate $(1 + \frac{16\kappa M}{N_B})^s$ by expanding the term up to second order in $\kappa M/N_B$ to give

$$Q_{\mathrm{QCB}} \approx \min_{0\leqslant s\leqslant 1}\left(1 + s(s-1)\frac{16\kappa^2 M}{2N_B}\right), \tag{19}$$

$$Q_{\mathrm{QCB}} \approx 1 - \frac{2\kappa^2 M}{N_B}. \tag{20}$$

We see from (19) that the minimum occurs at $s = 1/2$. Substituting the expression for Q_{QCB} in (1) gives an upper bound on the error probability,

$$p_{\mathrm{e}}^{(N)} \leqslant \frac{1}{2}\left(1 - \frac{2\kappa^2 M}{N_B}\right)^N \approx \frac{1}{2}e^{-2N\kappa^2 M/N_B}. \tag{21}$$

Comparing with the quantum Chernoff bound for quantum illumination using entangled photon pairs in the same parameter regime [8], we see a gain of a factor of 16 (i.e., 12-dB gain) in the probability error exponent for hyperentangled photon pairs. This result can be generalized to hyperentanglement in f degrees of freedom where we obtain a factor of 2^{2f} improvement in the exponent, provided each degree assumes only two discrete values. This result anticipates the improvement offered by hyperentanglement even in the high-noise regime, which is demonstrated by the performance analysis of the proposed receiver structure in the following sections. For the high-noise and low-signal-intensity regime, we consider the hyperentangled state obtained after (7) and (8) in the generation procedure, as opposed to the biphoton state considered in the low-noise regime.

III. HYPERENTANGLEMENT-ENHANCED OPA

The phase-sensitive cross correlations of the hyperentangled state are pivotal to the operation of the hyperentanglement-enhanced OPA (as well as the FF-SFG receiver). We explicitly calculate these phase-sensitive cross correlations,

$$\langle a_{3,H,S}a_{4,V,I}\rangle = \langle\Phi|\left(\frac{a_{1,H,S} + ia_{2,H,S}}{\sqrt{2}}\right)\left(\frac{ia_{1,V,I} + a_{2,V,I}}{\sqrt{2}}\right)|\Phi\rangle\,. \tag{22}$$

Observing that $\langle\Phi|\,a_{1,H,S}a_{2,V,I}\,|\Phi\rangle = \langle\Phi|\,a_{2,H,S}a_{1,V,I}\,|\Phi\rangle = 0$, the above equation can be further simplified,

$$\langle a_{3,H,S}a_{4,V,I}\rangle = \frac{i}{2}\langle\Phi|\,a_{1,H,S}a_{1,V,I}\,|\Phi\rangle + \frac{i}{2}\langle\Phi|\,a_{2,H,S}a_{2,V,I}\,|\Phi\rangle \tag{23}$$

$$= \frac{i}{4}\sum_{n=1}^{\infty}\frac{(N_S')^{n-1/2}}{(N_S'+1)^{n+1/2}}n + \frac{i}{4}\sum_{n=1}^{\infty}\frac{(N_S')^{n-1/2}}{(N_S'+1)^{n+1/2}}n \tag{24}$$

$$= \frac{i}{2}\sqrt{(N_S')(N_S'+1)}. \tag{25}$$

We can calculate $\langle a_{3,V,S}a_{4,H,I}\rangle$, $\langle a_{3,H,I}a_{4,V,S}\rangle$, and $\langle a_{3,V,I}a_{4,H,S}\rangle$ along similar lines with the result that all four phase-sensitive cross correlations possess an identical value, $\frac{i}{2}\sqrt{(N_S')(N_S'+1)}$. If we were to use a separable state instead of the hyperentangled state, then there would be either no initial correlations between the two spatial modes (for a direct product state) or the initial classical correlations would be much lower than entanglement-induced correlations with the

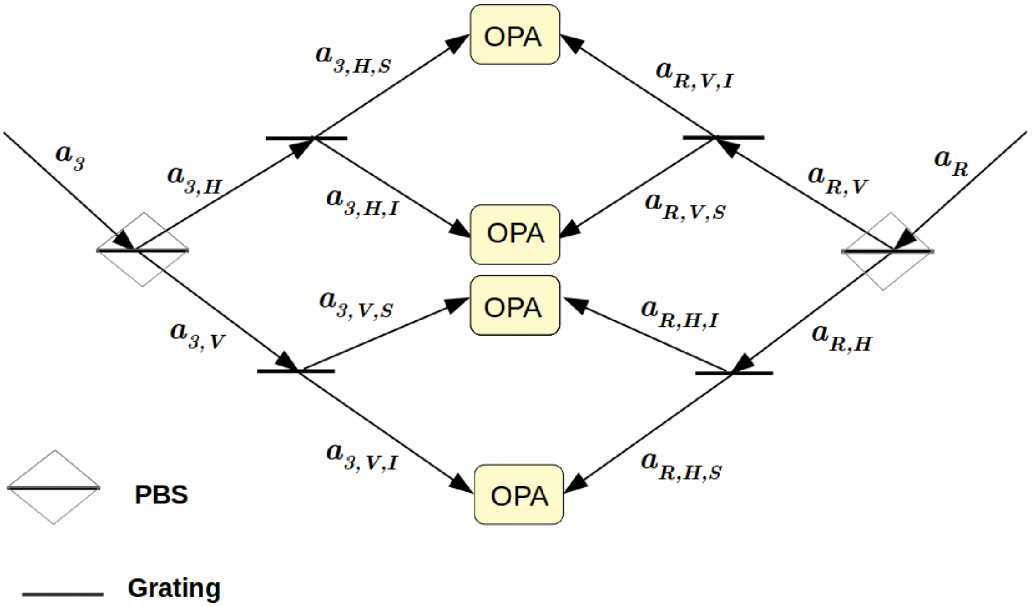

FIG. 1. Schematic representation of a hyperentanglement-enhanced OPA receiver. The stored spatial mode undergoes splitting by a polarizing beam splitter (PBS) and each of the two resulting modes are subjected to frequency-dependent splitting using optical grating. The returning state goes through an identical procedure. The four pairs of correlated modes form the inputs to four OPAs.

result that these correlations would deteriorate even further due to thermal noise. We exploit these correlations using a modified implementation of an OPA-based receiver [14], as demonstrated in the schematic representation in Fig. 1. One of the spatial modes, say 3, is stored, whereas the other spatial mode is dispatched towards the presumed target. In the absence of any object in the path, the returning mode a_R is simply the thermal bath mode a_B. When the object is present, the returning mode is of the form

$$a_R = \sqrt{\kappa} a_4 + \sqrt{1-\kappa} a_B. \tag{26}$$

In either case, the stored and the returning mode are subjected to two-level splitting, the first based on the polarization and the second based on the frequency, using a polarizing beam splitter and optical grating, respectively (see Fig. 1). As the thermal state is completely unpolarized, the thermal photons get divided equally between $a_{R,H}$ and $a_{R,V}$. Moreover, we may assume the thermal photons get distributed roughly equally between the signal and idler frequency modes if the two frequencies have a comparable magnitude. At the end of this splitting procedure, each of the four pairs forms the input to a type-II OPA having gain $G = 1 + \epsilon^2$, marginally greater than one. Let us consider the first of these parametric amplifiers with output c,

$$c = \sqrt{G} a_{3,H,S} + i\sqrt{G-1} a^{\dagger}_{4,V,I}. \tag{27}$$

This output is a thermal state with a mean photon number N_1 in the presence of the object and N_0 in its absence,

$$N_0 = G\frac{N_S'}{2} + (G-1)\Big(\frac{N_B}{4} + 1\Big), \tag{28}$$

$$N_1 = G\frac{N_S'}{2} + (G-1)\left(\frac{N_B}{4} + \kappa\frac{N_S'}{2} + 1\right) + \sqrt{G(G-1)\kappa N_S'(N_S'+1)}. \tag{29}$$

Such a distribution of photons [14] at an ideal photocounter will have variance $\sigma_m^2 = N_m(N_m+1)$, where m assumes the value of 1 or 0. The output of all four OPAs is identical in mean photon number and variance. A common photocounter is used to determine the photon count $N_{\rm pc}$ over all N transmitted temporal modes and the corresponding four amplifier outputs. The common counter needs to be positioned such that the output from each of the four amplifiers arrives at the counter sequentially. Alternately, four identical photocounters can be used for outputs of the four amplifiers. From classical detection theory [21], it follows that the threshold is $N_{\rm th} = 4N(\sigma_0 N_1 + \sigma_1 N_0)/(\sigma_0 + \sigma_1)$. When the photon number count $N_{\rm pc} > N_{\rm th}$, we declare the target to be present and vice versa. The error probability in detection $p^{(N)}_{{\rm e},H\text{-OPA}}$ is

$$p^{(N)}_{{\rm e},H\text{-OPA}} = \frac{1}{2}\mathrm{erfc}(2\sqrt{RN}) \leqslant \frac{e^{-4NR}}{4\sqrt{\pi NR}}, \tag{30}$$

where R is the signal-to-noise ratio,

$$R = \frac{(N_1 - N_0)^2}{2(\sigma_1 + \sigma_0)^2} \approx \frac{\kappa N_S}{4N_B}. \tag{31}$$

The final approximation is valid in the limit $N_S, \kappa, \epsilon \ll 1$ and $N_B \gg 1$. The signal-to-noise ratio for an ideal photocounter in our setup is half of that of the OPA receiver used for the TMSV probe. However, we have achieved a fourfold multiplicity in the number of readings for every iteration of the transmitter pulse, leading to a net 3-dB gain in the error exponent over a lone OPA receiver. In Fig. 2, we compare the performance of this receiver with earlier receiver models.

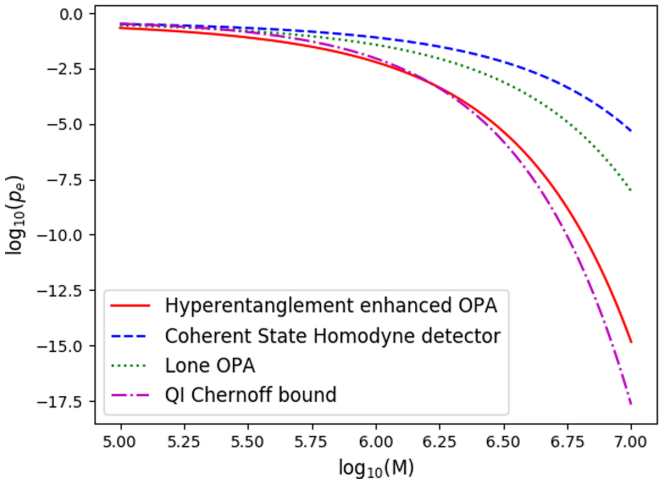

FIG. 2. Performance of different receivers. The error probability of detection for a hyperentanglement-enhanced OPA receiver is close to the QCB for TMSV and is therefore better than the coherent-state homodyne detector as well as the lone OPA receiver in the high-noise regime. The parameters used for the plots are $N_S = \kappa = 0.01$, $N_B = 25$, and $G = 1.005$.

IV. HYPERENTANGLEMENT-ENHANCED FF-SFG RECEIVER

If we replace each of the four OPA receivers with FF-SFG receivers, the resulting receiver setup outperforms the lone FF-SFG receiver. For a lone SFG receiver used in combination with N iterations of the TMSV probe state, the returning mode a_R and the idler mode a_I form the two inputs to give an output mode b whose frequency is the sum of the frequencies of the inputs. Due to practical considerations, K feed-forward cycles are carried out and the mean photon number of the SFG output at the end of each of the K cycles is determined. For a sufficiently large K and parameter regime, $\kappa \ll 1$, $N_S \ll 1$, and $N_B \gg 1$, the coherent contribution to the mean photon number in the absence of any object is nearly zero while in the presence of an object [16] it assumes the form

$$\sum_{k=1}^{K} \langle {b^{(k)}}^{\dagger} b^{(k)} \rangle = N |\langle a_R a_I \rangle|^2 / (1 + N_B) \approx \kappa N N_S / N_B. \quad (32)$$

Here, $b^{(k)}$ is the output at the end of kth cycle. The quantity in the preceding equation has been shown to be the exponent in the error probability bound for the FF-SFG receiver [16]. The error probability bound thus has the following form,

$$\sum_{k=1}^{K} \langle {b^{(k)}}^{\dagger} b^{(k)} \rangle = N |\langle a_R a_I \rangle|^2 / (1 + N_B) \approx \kappa N N_S / N_B. \quad (33)$$

The hyperentanglement-enhanced FF-SFG receiver model consists of four identical FF-SFG receivers which differ solely in their input modes. The input mode pairs for the four receivers following the hyperentanglement-based splitting procedure are $\{a_{3,H,S}, a_{R,V,I}\}$, $\{a_{3,V,S}, a_{R,H,I}\}$, $\{a_{3,H,I}, a_{R,V,S}\}$, and $\{a_{3,V,I}, a_{R,H,S}\}$. We focus on the first of these receivers with input modes $a_{3,H,S}$ and $a_{R,V,I}$. The error probability exponent for this receiver is calculated by replacing $|\langle a_R a_I \rangle|^2$ in (33) with $|\langle a_{3,H,S}, a_{R,V,I} \rangle|^2$ and N_B by $N_B/4$. This is because the thermal photons are distributed almost equally among the four modes $a_{R,V,I}$, $a_{R,H,I}$, $a_{R,V,S}$, and $a_{R,H,S}$ following the splitting procedure,

$$\langle a_{3,H,S} a_{R,V,I} \rangle \quad (34)$$

$$= \langle a_{3,H,S} (\sqrt{\kappa} a_{4,V,I} + \sqrt{1-\kappa} a_{B,V,I}) \rangle = \sqrt{\kappa} \langle a_{3,H,S} a_{4,V,I} \rangle \quad (35)$$

$$= \frac{i}{2} \sqrt{\kappa (N_S')(N_S' + 1)} = \frac{i}{2\sqrt{2}} \sqrt{\kappa (N_S)(N_S/2 + 1)}. \quad (36)$$

We have used the fact that $N_S' = N_S/2$. Substituting the above result in (33) and approximating the resulting expression under the conditions $N_S \ll 1$ and $N_B \gg 1$ yields

$$\sum_{k=1}^{K} \langle {b^{(k)}}^{\dagger} b^{(k)} \rangle = \frac{\kappa N N_S (N_S/2 + 1)}{8(1 + N_B/4)} \approx \kappa N N_S / 2 N_B. \quad (37)$$

The error probability is therefore bounded as follows,

$$p_{\mathrm{e},1}^{(N)} \leqslant e^{-\kappa N N_S / 2 N_B}. \quad (38)$$

The subscript 1 in the error probability indicates the first of four FF-SFG receivers. The total error probability is given by

$$p_{\mathrm{e}}^{(N)} = \prod_{i=1}^{4} p_{\mathrm{e},i}^{(N)} \quad (39)$$

As the phase-sensitive correlations appearing in the exponent of the error probability for each receiver are identical, it follows that

$$p_{\mathrm{e}}^{(N)} = \left(p_{\mathrm{e},1}^{(N)}\right)^4 \leqslant e^{-2\kappa N N_S / N_B}. \quad (40)$$

We see a factor-of-2 (i.e., 3-dB) improvement in the exponent over the performance of a lone FF-SFG receiver. Thus, the hyperentanglement-enhanced FF-SFG receiver outperforms the optimal quantum illumination receiver by 3 dB in the error probability exponent.

V. CONCLUDING REMARKS

In this article, we have shown the benefits of hyperentanglement in the low-noise as well as high-noise regime with a 12-dB improvement over QI in the low-noise regime and two variants of a hyperentanglement-enhanced receiver in the high-noise regime matching the FF-SFG receiver performance in one instance and surpassing it in the other. The main advantages of the receiver model proposed in this article stem from the distribution of thermal noise photons into four modes following the splitting procedure. Hyperentanglement enables us to achieve such a distribution without nullifying the phase-sensitive cross correlations. For the probe state considered, the performance of the proposed receivers is (possibly) suboptimal and only a complete Chernoff bound computation of the hyperentangled probe states using symplectic decomposition will shed light on the optimal performance [22]. However, it should be noted that despite possibly being suboptimal, the hyperentanglement-enhanced FF-SFG receiver outperforms the lone FF-SFG receiver, making it the best receiver model to date. The hyperentanglement-based splitting procedure in our

model is general enough to allow for other degrees of freedom such as the time bin to replace the polarization or frequency in order to circumvent any practical issues associated with the frequency and polarization of hyperentangled states. In fact, if we are able to exploit entanglement in a third degree of freedom we will be able to surpass the performance of the hyperentanglement-enhanced OPA by 3 dB. In conclusion, the proposed receiver structure is highly versatile and lends itself to several modifications that need to be further investigated.

ACKNOWLEDGMENTS

A.V.P., B.S., and C.M.C. acknowledge the support of Kishore Vaigyanik Protsahan Yojana (KVPY), Infosys Young Investigator grant, and Ramanujan Fellowship, respectively.

[1] S. Pirandola, B. R. Bardhan, T. Gehring, C. Weedbrook, and S. Lloyd, Nat. Photonics **12**, 724 (2018).
[2] J. H. Shapiro, IEEE Aerosp. Electron. Syst. Mag. **35**, 8 (2020).
[3] C. W. Helstrom and C. W. Helstrom, *Quantum Detection and Estimation Theory* (Academic, New York, 1976), Vol. 3.
[4] K. M. R. Audenaert, J. Calsamiglia, R. Munoz-Tapia, E. Bagan, L. Masanes, A. Acin, and F. Verstraete, Phys. Rev. Lett. **98**, 160501 (2007).
[5] S. Lloyd, Science **321**, 1463 (2008).
[6] S.-H. Tan, B. I. Erkmen, V. Giovannetti, S. Guha, S. Lloyd, L. Maccone, S. Pirandola, and J. H. Shapiro, Phys. Rev. Lett. **101**, 253601 (2008).
[7] In a high-noise, low-signal-intensity, and high-loss regime, the quantum Chernoff bound for coherent states is $e^{-\kappa N_S/4N_B}/2$. This bound is saturated using a homodyne detector.
[8] J. H. Shapiro and S. Lloyd, New J. Phys. **11**, 063045 (2009).
[9] M. F. Sacchi, Phys. Rev. A **71**, 062340 (2005).
[10] P. G. Kwiat, J. Mod. Opt. **44**, 2173 (1997).
[11] F.-G. Deng, B.-C. Ren, and X.-H. Li, Sci. Bull. **62**, 46 (2017).
[12] S. P. Walborn, A. H. Pimentel, L. Davidovich, and R. L. de Matos Filho, Phys. Rev. A **97**, 010301(R) (2018).
[13] C. Chen, A. Riazi, E. Y. Zhu, and L. Qian, Phys. Rev. A **101**, 013834 (2020).
[14] S. Guha and B. I. Erkmen, Phys. Rev. A **80**, 052310 (2009).
[15] Z. Zhang, S. Mouradian, F. N. C. Wong, and J. H. Shapiro, Phys. Rev. Lett. **114**, 110506 (2015).
[16] Q. Zhuang, Z. Zhang, and J. H. Shapiro, Phys. Rev. Lett. **118**, 040801 (2017).
[17] J. T. Barreiro, N. K. Langford, N. A. Peters, and P. G. Kwiat, Phys. Rev. Lett. **95**, 260501 (2005).
[18] P. G. Kwiat, E. Waks, A. G. White, I. Appelbaum, and P. H. Eberhard, Phys. Rev. A **60**, R773 (1999).
[19] The generation of the described states is experimentally challenging but since $N_S' \ll 1$, the predominant contribution stems from the vacuum state and a pair of photons. So, the states, under a first-order approximation, behave as polarization-entangled states which are routinely generated in laboratories.
[20] J. Calsamiglia, R. Muñoz-Tapia, L. Masanes, A. Acin, and E. Bagan, Phys. Rev. A **77**, 032311 (2008).
[21] E. L. Lehmann and J. P. Romano, *Testing Statistical Hypotheses* (Springer, Berlin, 2006).
[22] S. Pirandola and S. Lloyd, Phys. Rev. A **78**, 012331 (2008).